An expanded state diagram for the directed self-assembly of colloidal suspensions in toggled fields

Hojin Kim, Moujhuri Sau, and Eric M. Furst*

Department of Chemical and Biomolecular Engineering, Allan P. Colburn Laboratory, University of Delaware, Newark, DE 19716, United States

E-mail: furst@udel.edu

Abstract

The suspension structure and assembly kinetics of micrometer-diameter paramagnetic spheres in toggled magnetic fields are investigated at a constant field strength $H = 1750$ Am^{-1} while toggling the field on and off over the frequency range $0.3 < f < 5$ Hz and duty ratio values (the fraction of time the field is on over one toggle period) $0.05 \leq \xi \leq 0.8$. Five microstructures form after sufficient time in the toggled field: fluid, columnar, percolated, ellipsoidal-shaped, and perpendicular, and their kinetic pathways are identified. For ellipsoidal-shaped microstructures, diffusion-driven particle aggregation at early times gives way to a fluid-like breakup. For columnar- and percolated-structures, this coarsening arrests before breakup. As the toggling duty cycle decreases, the range of frequencies for each structure narrows, giving way to an unstructured fluid; below $\xi < 0.1$, only the fluid state is observed. The existence of fluid, columnar, percolated, and ellipsoidal-shaped microstructures agree well with those predicted by the theoretical and computational work of Sherman et al. (Z. M. Sherman, H. Rosenthal, J. W. Swan, Langmuir **34**, 1029–1041, 2018). Microstructures that connect perpendicularly to the magnetic field are identified for $0.1 \leq \xi \leq 0.3$ and $1.6 < f < 3.7$ Hz. Perpendicular microstructures also exhibit emergent dynamics with continuous rotation, breakup, and coalescence events.

Introduction

Colloidal assembly is a promising approach for creating ordered micro- and nano-structured materials in a highly scalable process.[1] Examples of assembled colloidal materials include photonic[2–4] and phononic[5–7] crystals, inverse opals for size-selective filtration,[8–10] and sensors.[11,12] Colloids can self-assemble – naturally, in the case of gem opals[13,14] – due to the hard-sphere crystallization transition[15] and also by tailoring interparticle interaction potentials through the use of externally-applied fields,[16–18] DNA hybridization,[19–22] and depletion interactions.[23,24]

Field-directed self-assembly is a straightforward way to control the interaction potential and structure of colloidal suspensions. Suspensions of polarizable colloids, in which the dipole-dipole interaction is induced by an external electric or magnetic field, typically form gel-like microstructures as the particles align and form chains parallel to the applied field in early stages of assembly.[25,26] Later, these chains interact laterally to form thicker, percolated fibrous structures.[27] While such microstructural changes give rise to rapid and reversible transitions of electro- and magneto-rheology,[28,29] the kinetically-arrested structure under steady fields generally prevents the sus-

pension from forming ordered, equilibrium particle arrays.[30–32]

In an effort to circumvent the kinetically-arrested state in an external field, Promislow and Gast first made use of toggling, in which the field is turned on and off periodically with a square waveform at a frequency f.[33,34] In a toggled magnetic field, paramagnetic colloidal suspensions reach an energetic minimum through the formation of large, spiky ellipsoidal-shaped domains oriented with the field[33,34] Later, Swan and coworkers studied the kinetics of this microstructural transition.[35,36] The growth of the magnetic particle domain width with time $\langle s(t)\rangle$ followed an initial power-law behavior $\langle s(t)\rangle \sim t^z$ with exponents $z \sim 0.3$ due to either a diffusion-limited surface or bulk diffusion coarsening mechanism.[37] At longer times, the depercolation and the coalescence processes cause a rapid growth of the microstructure, which results in a cross-over of the coarsening exponent to super-unity values, $z \sim 1.5$.

These previous experimental studies focus on the effect of toggled fields at a constant duty ratio $\xi = 0.5$. Here, $\xi = t_{on}/(t_{on} + t_{off})$ is the ratio of field-on time duration (t_{on}) in one toggling cycle period $t_{on} + t_{off} = 1/f$, where t_{off} refers to field-off time duration and f is the toggling frequency. Recent computational and theoretical studies by Sherman and coworkers suggest that varying toggling parameters (f and ξ) affects the self-assembly kinetics, rate, and mechanisms, as well as enhances the final crystallinity of the self-assembled structure.[38–40]

An experimental investigation of the structures in magnetic colloidal suspensions as a function of duty ratio and toggling frequency is still lacking, despite a wide range of applications that would benefit from possibly faster growth rates and robust organization into defect-free crystalline states. In this article, we address this need by studying paramagnetic colloids assembled in toggled magnetic fields. The self-assembly kinetics are measured by observing changes in the suspension microstructure with time. Microstructures are mapped onto a state diagram and the correlation between the structural phase and the growth kinetics is

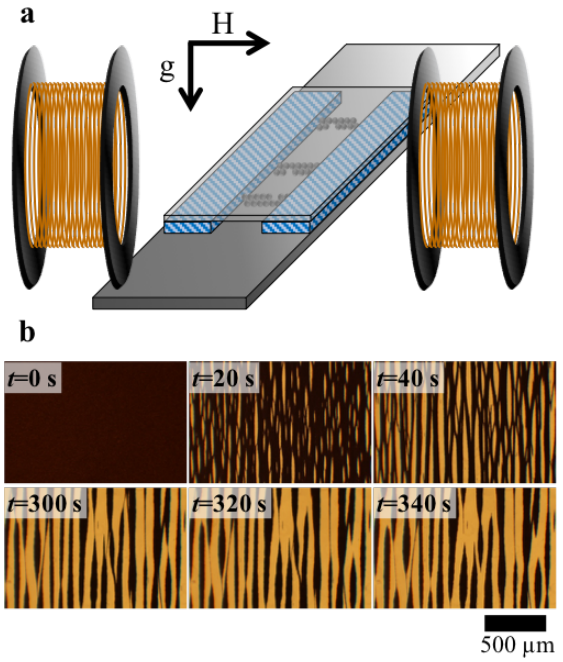

Figure 1: **(a)** Experimental setup for magnetic particle self-assembly. **(b)** Optical microscope images show phase-separation and microstructure formation of self-assembling colloidal particles at $f = 1$ Hz and $\xi = 0.35$. Scale bar: 500 μm.

made. Interestingly, we identify a narrow region of frequencies and duty ratios in which a new class of perpendicular microstructures form with wavy-shaped patterns that connect perpendicular to the applied field.

Material and Methods

Paramagnetic colloid suspensions

The magnetic suspensions are polystyrene particles containing iron oxide superparamagnetic nanoparticles (diameter $2a = 1.05$ μm, magnetic susceptibility $\chi = 1.4$, saturation magnetization $M_{\text{sat}} \approx 4 \times 10^4$A/m, Dynabeads My-One). The particles are dispersed in ultra-pure water (resistivity >18.2 MΩ·cm) at a volume fraction $\phi = 5 \times 10^{-3}$. A glass slide and a coverslip are sandwiched with a spacer of two 100 μm thick rectangular double-sided adhesive strips. The particle suspension is introduced by capillary action into the rectangular cross-section channel. Due to the high density mismatch between water and the particles (particle density, $\rho_p = 1.8$ mg·mL^{-1}), the colloids sediment and initially form a uniform monolayer with approximately 75% surface area coverage before the experiment commences.

Self-assembly in toggled fields

For each self-assembly experiment, the sample is placed on an inverted optical microscope (Zeiss Axio Observer) at the center of a Helmholtz coil, which generates a magnetic field perpendicular to the gravity and in the sample plane (cf. Figure 1a). The magnetic field is applied and toggled on and off in a square-wave with controlled duty ratio ξ and frequency f using a function generator (Agilent 33220A) and three power transistors (IRF 840) connected in parallel as the current switch for a DC power supply (BK Precision 1621A). All of the experiments in this work are performed by toggling between $H = 1750$ A·m^{-1} and 0 A·m^{-1}.

The interactions between the paramagnetic particles are characterized by the induced dipole strength

$$\lambda = \frac{\pi \mu_0 a^3 \chi^2 H^2}{9 k_{\text{B}} T}, \tag{1}$$

which is the ratio of the maximum field-induced attraction between the particles to the thermal energy. Here, k_{B} is the Boltzmann constant, T the absolute temperature, μ_0 the vacuum permeability, a the particle radius, and H the magnetic field strength generated by the coils in the imaging region. The magnetic field strength is in the linear magnetization regime of the particles and well below their saturation magnetization. The corresponding dipole strength for the field strength $H = 1750$ A·m^{-1} is $\lambda \approx 93$.

After starting the toggling, the suspension is imaged at regular intervals (1 frame / second) under Kohler bright-field illumination using a digital camera (Canon EOS Rebel T2i). Representative images of the the suspension for $f = 1$ Hz, $\xi = 0.35$, and magnetic field strength $H = 1750$ A·m^{-1} are shown in Figure 1b.

Small-angle light scattering (SALS) experiments are performed with a laser of a wavelength $\lambda = 635$ nm (Edmund Optics, Stock #54-023). The laser passes through an aperture with a 1 mm diameter before being reflected by a mirror placed below the sample on the microscope stage. A screen is placed 2.75 cm above the sample and imaged with a camera. The SALS setup provides a wavevector range q between 1.3 and 9.5 μm^{-1}.

Results and Discussion

In the following results and discussion, we present the effect of the toggled field duty cycle on the suspension microstructure in three sections: first, we discuss the steady-state or "terminal" microstructure of the suspension after a long period of toggling. The toggling duration depends on the coarsening kinetics, which are discussed second. Third, we present further details of a new subset of microstructures, dynamics, and kinetics observed for a narrow range of duty ratios and frequencies, which we call the perpendicular microstructure.

Steady-state suspension structure and state diagram

Representative images of the suspension microstructure are shown in Figure 2 for each toggle frequency and duty cycle. We observe four general structures: columnar, ellipsoidal, percolated, and perpendicular-shaped. These are identified in the figure by green, blue, orange, and red outlines. Columnar, ellipsoidal, and percolated structures are similar to those reported in previous studies at a single duty ratio $\xi = 0.5$.[36,41,42] The wavy-shaped perpendicular structures are unique to this work and are discussed in detail later.

Suspensions in all of the toggled-field conditions exhibit some amount of coalescence into concentrated particle domains and subsequent coarsening. For columnar and percolated structures, the coarsening slows and eventually arrests. Under other toggle conditions, the particle domains break up into finite-sized "ellipsoidal structures" aligned in the direction of the magnetic field. The ellipsoidal shapes form via a Rayleigh-Plateau instability.[41,42] The occurrence of the Rayleigh-Plateau instability confirms that particles do not form a two dimensional structure, but generate a flattened 3D structure. The wavelength of the instability enables one to estimate an effective viscosity of the particle-dense domain as reported by Bauer and coworkers.[41] Percolated and columnar structures occur at the highest and lowest toggle frequencies, respectively.

The toggle duty cycle affects the final suspension microstructure by shifting the transition frequency between the columnar, ellipsoidal, and percolated states. At the duty cycle $\xi = 0.35$, breakup into ellipsoids occurs in a narrower range of frequencies, while at the lowest toggle duty cycle, $\xi = 0.1$, no breakup occurs at all.

Small-angle light scattering (SALS) is used to characterize the suspension structure on the lengthscale of the particles. Representative SALS scattering patterns are shown in Figure 3 for a homogeneous suspension, fluid, percolated, columnar, ellipsoidal, and perpendicular structures. An isotropic pattern of a suspension in the absence of an applied field indicates that particles are homogeneously distributed. After applying the toggled magnetic field, the scattering patterns at the lowest scattering vectors q become anisotropic due to the orientation of the assembling particles parallel to the field direction. At higher scattering vectors, the fluid, percolated, ellipsoidal, and perpendicular structures exhibit distinct peaks with a six-fold symmetry that indicates local crystallinity in the condensed phases. The radial peak positions correspond to the average distance between the particles, $1.4d$. The peaks are smeared for the fluid and percolated structures, and sharper for ellipsoidal and perpendicular states. The columnar structure lacks such peaks entirely, indicating a disordered structure at the particle level. The absence of crystallinity for the columnar structure agrees well that of a metastable fluid/fluid coexistence phase observed in Brownian dynamics simulations.[40] We will return to comparisons with the computational studies in more detail below.

State diagram. The final microstructures are organized into the state diagram shown in Figure 4a with representative images in Figure 4b. Each state is represented by the value of t_{off} and duty ratio $\xi = t_{\text{on}}/(t_{\text{on}} + t_{\text{off}})$. We use the characteristic time required for a particle to diffuse a distance equal to its radius in a solvent with viscosity η, $\tau_{\text{D}} = 6\pi\eta a^3/k_{\text{B}}T$ to scale t_{off}. Isofrequency lines are also plotted in the figure to highlight the other controlling experimental parameter after the duty ratio.

A fluid-like, non-condensed phase (black crosses) occurs at the lowest duty ratios $\xi < 0.1$ or at a high toggling frequency $f > 20$ Hz, as the pulse width t_{on} when the field is on is too short to drive particle aggregation. An increase in t_{off}, corresponding to the decrease of the frequency, at $0.04 < t_{\text{off}}/\tau_{\text{D}} < 1$ leads to a t_{on} long enough to form particle-condensed microstructures. However, the condensed particles do not relax and reorganize when t_{off} is shorter than τ_{D}, and therefore the suspension arrests in the percolated microstructure (orange region).

For $t_{\text{off}}/\tau_{\text{D}} \sim 1$, represented by the blue region and symbols in Figure 4a, the particles rearrange repeatedly and the microstruc-

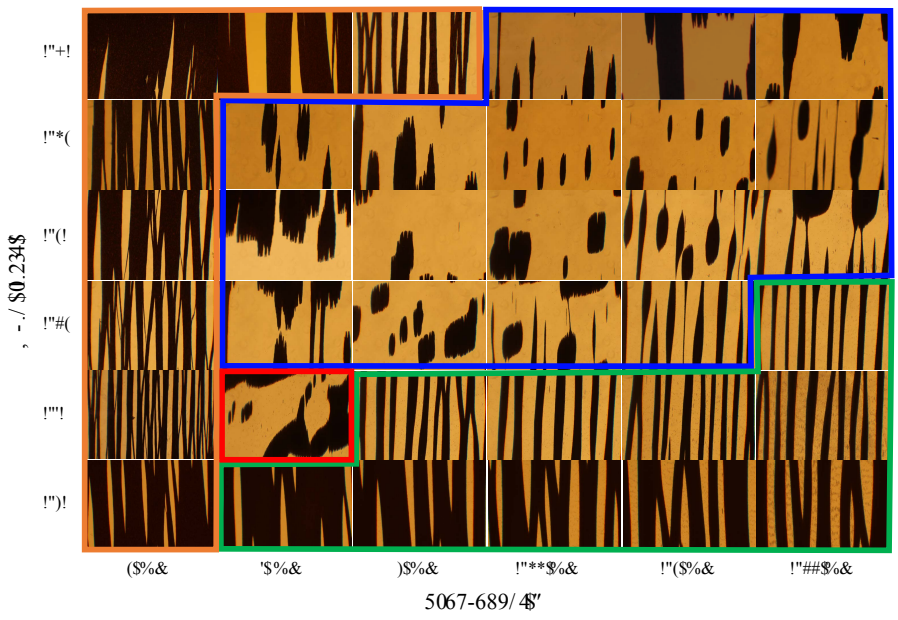

Figure 2: Bright-field optical micrographs of the suspension microstructure. Toggled frequency (f) and duty ratio (ξ) are varied at a constant field strength $H = 1750$ A·m^{-1}. Green, blue, orange, and red boundaries refer to columnar, ellipsoidal, percolated, and perpendicular microstructures, respectively. The dimensions of each image are 1.5 mm × 1 mm.

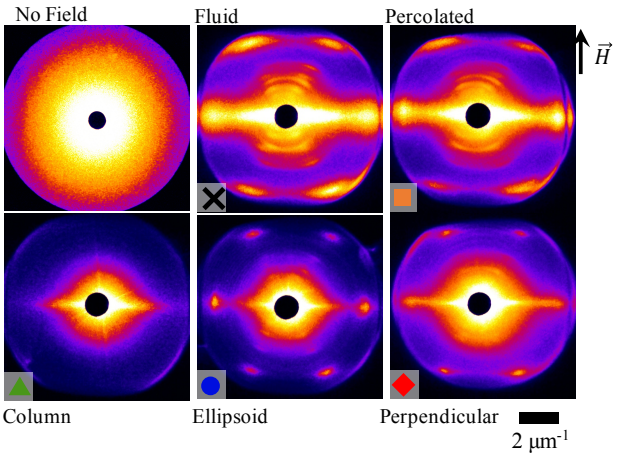

Figure 3: Representative small angle light scattering patterns for a homogeneous suspension, fluid, percolated, columnar, ellipsoidal, and zigzag-shaped perpendicular structure in the toggled field strength $H = 1750$ A·m^{-1}. The field direction is oriented from the bottom to top in each image. Scale bar: 2 μm^{-1}

ture evolves towards a thermodynamically more favorable state of ellipsoidal-shaped domains through a Rayleigh-Plateau breakup. As ξ decreases, the range of $t_{\rm off}/\tau_{\rm D}$ values where ellipsoids form also decreases. Instead, the structure arrests into columns (green symbols). This dependence of the microstructural state on duty ratio can be attributed to $t_{\rm off}$ being few times longer than $\tau_{\rm D}$. When the field-off time duration is too long, particles diffuse outside the range of the capture radius ($r_{\rm c}$), the distance between particles to have interaction potential of $1k_{\rm B}T$, that can be defined as $r_{\rm c} = (8\pi\mu_0 a^6\chi^2 H^2/9k_{\rm B}T)^{1/3} = 2a\lambda^{1/3} \approx 8.6a$.[36] In the case of $t_{\rm off} > r_{\rm c}$, particles are no longer bound in the aggregated microstructure and the colloidal suspension coarsening kinetics slow. However, some conditions near the boundary between the ellipsoidal- and the columnar-structure state show slow growth kinetics at the late-stage of self-assembly. In this respect, these structures are intermediate states that may evolve into ellipsoidal structures given enough time.

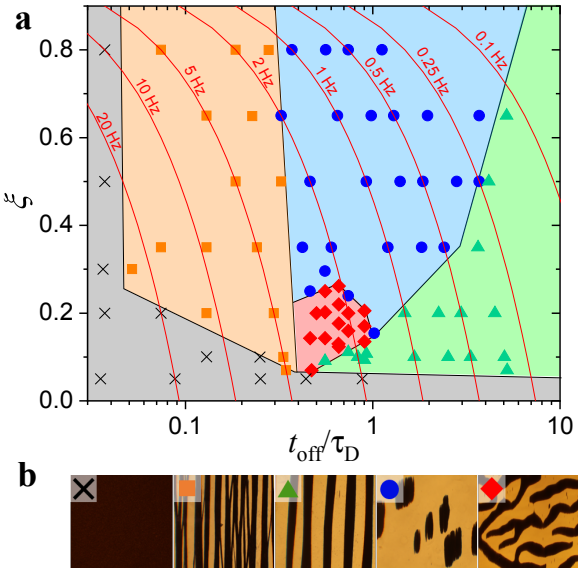

Figure 4: Microstructure state diagram. **(a)** Final microstructures for fluid-like (black crosses), percolated (orange squares), ellipsoidal (blue circles), columnar (green triangles), and perpendicular (red diamonds) structures are mapped into the diagram as duty ratio $\xi = t_{on}/(t_{on} + t_{off})$ versus t_{off}/τ_D. The red solid lines are isofrequency lines. **(b)** Corresponding images of the colloidal microstructures.

The newly-identified phase of perpendicular microstructures is observed within the range of parameters $0.5 < t_{off}/\tau_D < 1$ and $0.1 < \xi < 0.2$, shown as the red regime in Figure 4a (see also $f = 2$ Hz and $\xi = 0.2$ in Figure 2).

Except for the perpendicular phase, the experimental state diagram is nearly identical to the phase diagram for particle assembly with toggled interactions between polarizable particles computed by Brownian dynamics simulations.[40] (Figure S1 in the Supporting Information presents the phase diagram reported previously next to the experimental results.) In the Brownian dynamics simulations, mutually polarizable colloids are modeled to calculate the equilibrium phase diagram of suspension. The inclusion of mutual polarization incorporates both the external magnetic field and the local induced field of the particles. Such a particle-level simulation captures the interfacial energy, osmotic pressure, and inter-domain interactions that have been described in a domain-level manner by Cutillas and coworkers.[43] In the Brownian dynamics simulations presented by Sherman and Swan,[39,40,44] hydrodynamic interactions are not taken into account; however, Fiore and Swan confirmed that there are no qualitative changes in the results by performing Brownian dynamics simulations with and without hydrodynamic interactions.[45]

In both the experiments and simulations, comparable phases (fluid, columnar, percolated, and ellipsoidal structures) are observed. The resemblance of the phase boundaries between experiments and simulations is noteworthy; a fluid phase occurs at $\xi < 0.1$; percolated structures occur at low values of t_{off}/τ_D, columns at high values, and ellipsoids at intermediate to the two with a range of t_{off}/τ_D that increases with increasing duty ratio. However, the simulation phase boundary is quantitatively shifted towards lower t_{off}/τ_D values. This difference may be attributed to the strength of the polarizable interaction in our experiments or the geometry of the samples. The field strength $\widetilde{H}_{0,\text{experiment}} = 11.6$ is used in the experiments, whereas $\widetilde{H}_0 = 3$ is the highest value with a phase diagram reported for the simulations. Here, $\widetilde{H}_0 = H_0\sqrt{a^3\mu_f \text{f}/k_B T}$ with the sol-

vent permeability μ_f. The geometry of the experiments is also different. The experiments are performed in a gravitational field, which adds another contribution to the suspension energy[46] and pushes the aggregates into close proximity with a solid interface. Thus, it would not be surprising if the hydrodynamic interactions contributed to the apparently slower dynamics,[47] although microgravity experiments have produced results that are similar to ground-based experiments.[35]

Effect of duty cycle on the coarsening kinetics

We analyze the microstructure growth kinetics by calculating the power spectrum of the time series of microscopy images. Micrographs taken every 20 s at a given toggling condition are used to calculate the power spectral density along direction perpendicular to the applied magnetic field. The peak position is fitted at the maximum intensity (I_{max}) and the corresponding wavevector (q_m) is plotted with the time after applying the toggling field in Figure 5a and 5b. The q_m and time t axes are normalized by the wavevector q_c at the corner time t_c at which the growth kinetics exhibit a change in scaling. The wavevector q_m represents the characteristic length scale (L_c) of the microstructures with the relation $L_c = 2\pi/q_m$. Therefore, the power-law behavior of structural growth can be seen as $q_m \sim \langle s(t)\rangle^{-1} \sim t^{-z}$.

The suspensions follow one of two kinetic pathways after a period of similar initial coarsening. The two paths are distinguished by whether the microstructures condense into finite-length domains or eventually arrest as either columns or percolated structures (e.g. states green or orange). For ellipsoidal microstructures shown in Figure 5a, the coarsening initially conforms the power-law behavior with $q_m \sim t^{-0.25}$ or $t^{-0.33}$, which corresponds to surface diffusion- or bulk diffusion-mediated structural growth, respectively.[37] The late-stage growth kinetics undergo a crossover of z from sub-unity to a super-unity exponent $z \geq 1.5$, which indicates faster growth of the characteristic size scale of microstructures.[35,36,48]

The growth kinetics of percolated and columnar structures in Figure 5b differs from the ellipsoidal-shaped structures primarily at their late stages. After the initial coarsening, which follows similar power-law kinetics, the structural growth eventually stops, indicating the absence of (or undetectably slow) inter-domain coalescence or breakup.

The coarsening exponent z before the breakthrough time is shown as a function of duty ratio ξ in Figure 5c. The exponent does not exceed the bulk-diffusion dominant growth rate $z_{bulk} = 1/3$ and generally, $z_{surf} < z < z_{bulk}$ where $z_{surf} = 1/4$ is the exponent for the surface diffusion growth.

All of the corner times t_c for the breakup events (Figure 5d) are in a good agreement with the previous study performed at a constant duty ratio $\xi = 0.5$.[36] This breakthrough time t_c increases exponentially and it can be scaled as $\exp[(0.92\text{ s})f]$ for $f > 1$ Hz; the coefficient is comparable to the diffusive time scale of the particles $\tau_D \sim 0.92\text{s}^{-1}$. At low frequencies, e.g. $f < 1$ Hz, the condensed state formed during the field-on stage is partially lost due to the particles diffusion further than the capture radius of the interaction potential. This loss of structure requires more cycles to generate the break-up process and leads to a steep increase in breakthrough time that consistent with the approximation $t_c \sim \exp[-(7.9\text{ s})f]$ introduced in the earlier study.[36]

Growth and dynamics of the perpendicular structure

This work identifies a new state, which we call "perpendicular", identified as the red region in Figure 4. It has a final microstructure that connects orthogonally to the magnetic field and occurs in a narrow range of toggle frequencies and duty ratios: $1.6 < f < 3.7$ Hz and $0.1 \leq \xi \leq 0.3$. Here, we discuss the perpendicular structure in more detail, including its growth kinetics and dynamics.

Structural evolution. The growth and breakup process for the perpendicular structure are shown in Figure 6a. Instead of a homo-

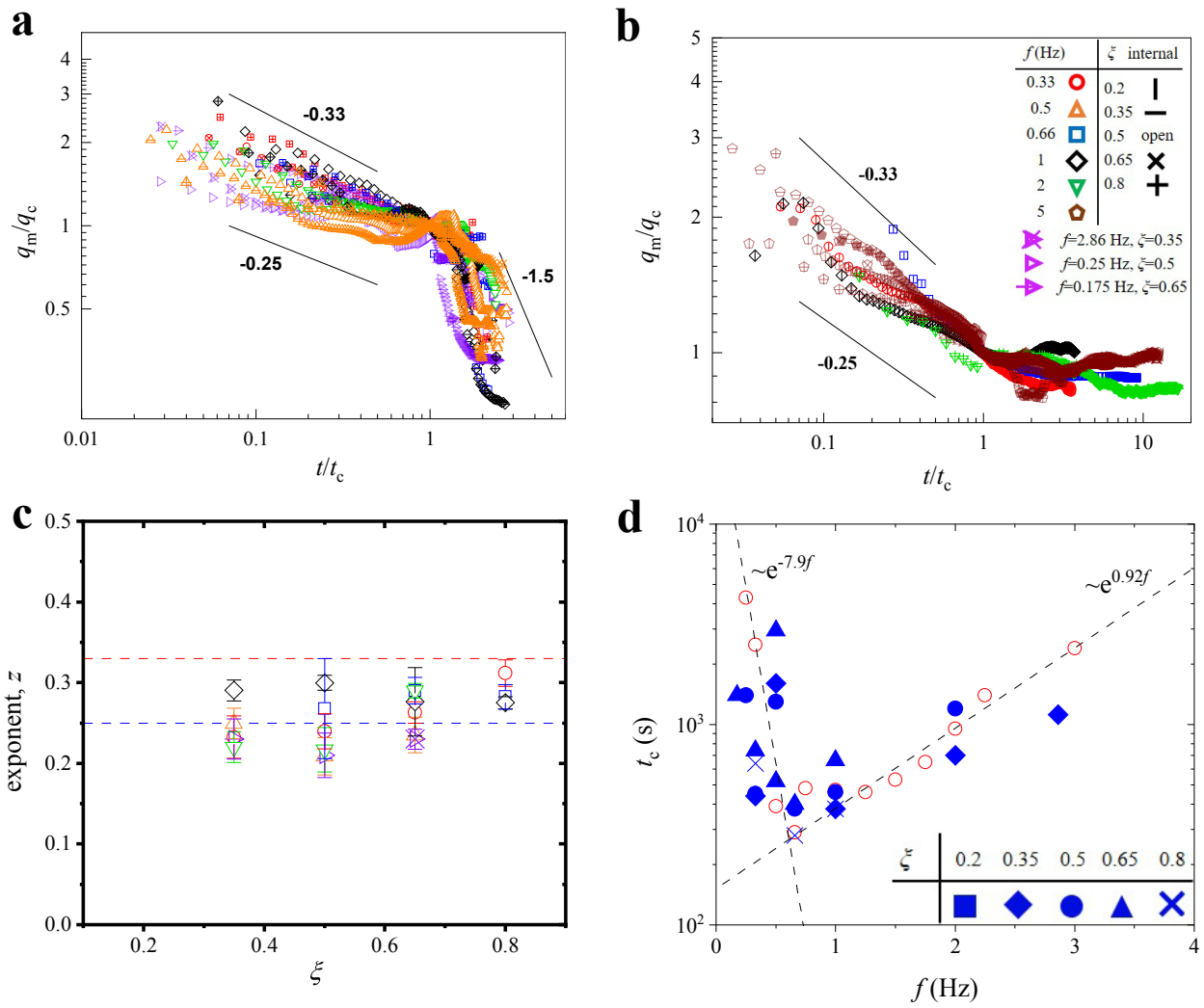

Figure 5: The microstructure growth kinetics of **(a)** ellipsoidal-shaped (conditions within a blue boundary in Figure 2), **(b)** percolated and columnar structures (orange and green boundaries in Figure 2). The maximum intensity peak wavevector (q_m) is shown versus time (t) normalized by the critical wavevector (q_c) and the critical time (t_c) referring to values at a crossover. The black solid lines are reference slopes. An inset table on the *top right* of **(b)** shows symbols used in **(a)** and **(b)**. **(c)** Exponents at early stage in the ellipsoidal microstructure formation plotted as a function of duty ratio ξ at toggled frequencies f=0.33 (blue rectangle), 0.5 (red diamond), 0.66 (black circle), 1 (green triangle), and 2 Hz (magenta cross). Red and blue dashed lines indicate exponents for diffusion ($z = 1/3$) and surface diffusion ($z = 1/4$) dominant aggregation, respectively. **(d)** The critical time is plotted as a function of frequency (f) for the ellipsoidal state (blue symbols). Red circles are exported from the previously reported data.[36]

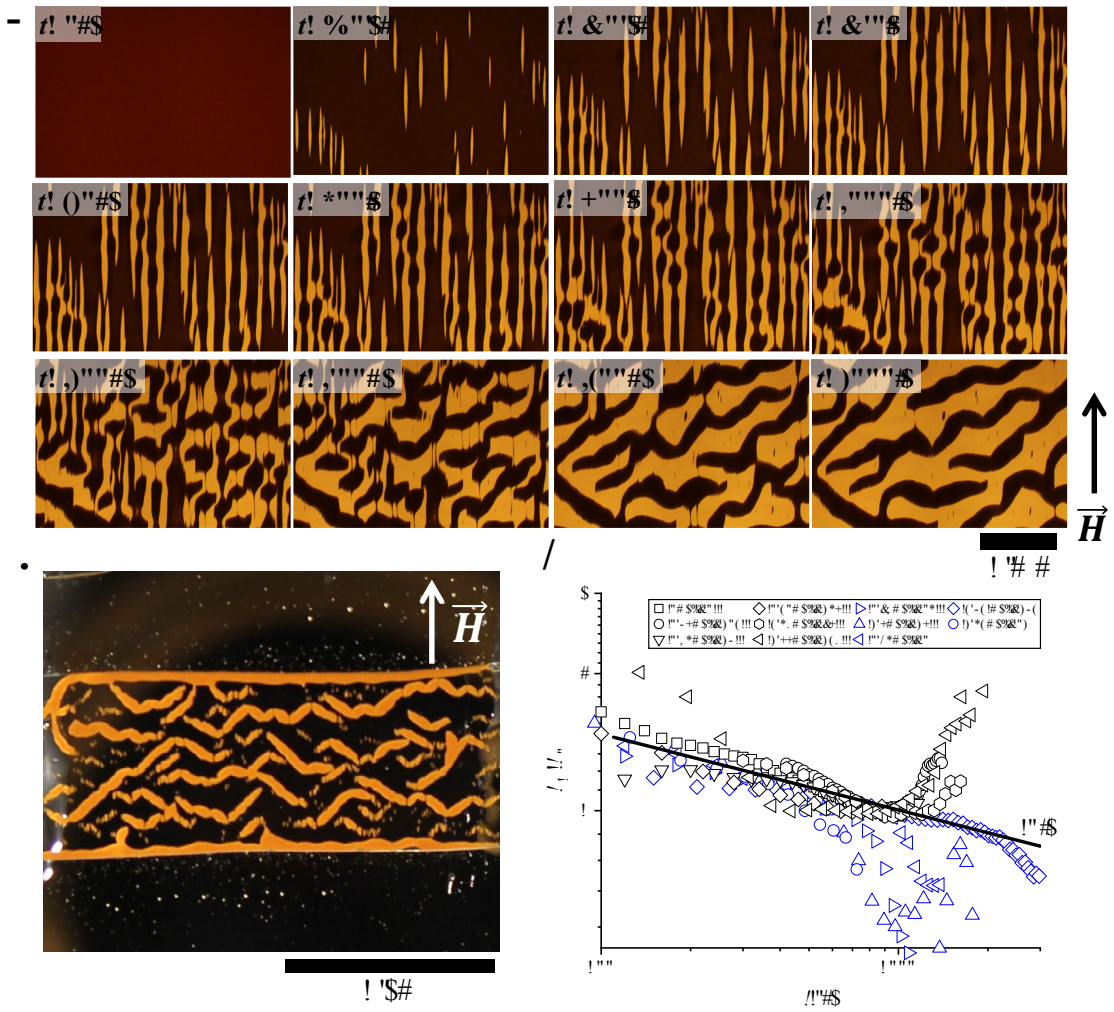

Figure 6: **(a)** The growth of the perpendicular structure in the toggled field of $f = 2.47$ Hz and $\xi = 0.124$ over time in bright-field images is presented. A low magnification image is in **(b)**. The bright area in **(b)** corresponds to the particle-rich domain. Arrows indicate the applied field direction. **(c)** Microstructure growth kinetics of the perpendicular structure are characterized as the maximum wavevector of the structure perpendicular to the field normalized by the wavevector at the curve's inflection, q_m/q_c with time t. Curves with an initial downwards inflection before turning upwards are denoted by blue symbols, while those that turn upwards are shown in black. The black solid line is a logarithmic slope of -1/6. Scale bar: 1 mm in **(a)** and 1 cm in **(b)**.

geneous aggregation of percolated, column-like structures (cf. Figure 7b), at the start of toggling, voids that are empty of particles nucleate sparsely throughout the suspension. The voids grow, forming thick, but percolated columns by $t = 600$ s and later, the deformation becomes more apparent and begins to break up around $t = 1000$ s. However, instead of forming isolated aggregates, the nascent structures coalesce laterally (e.g. at $t = 1200$ s) and finally, the colloidal suspension forms a connected, alternating pattern perpendicular to the applied magnetic field. The perpendicular structure can span centimeters, as shown by the low magnification image in Figure 6b.

In Figure 6a, we plot the maximum wavevector perpendicular to the field of the developing microstructure with time. Two distinguishable sets of curves emerge, indicated by black and blue symbols. In the first first set (black symbols), q_m decreases before turning upwards. This increase after the suspension initially coarsens reflects the micrograph sequence discussed above: the aggregate widths decrease by forming zig-zag pattern directly from the thick percolated networks. In the second set (blue symbols), q_m exhibits an initial and more rapid downturn, as if approaching a breakthrough similar to the growth at the ellipsoidal state, but then turns upwards as the perpendicular state forms. A proximity to the state boundary differentiates the two sets of curves. The experiments represented by the blue symbols lie near the perpendicular-ellipsoidal state boundary in Figure 4a.

The downturn followed by an upturn of q_m in the experiments close to the state boundary may reflect a competition of timescales, since the onset of the downturn varies with the state point conditions. Interestingly, the wavevector decreases as a power law scaling with time $q_m \sim t^{-z}$ for all of the perpendicular states, with a dependence similar to those observed for the early-stages of spinodal decomposition, $z = 1/6$.[49,50] One state-point in particular is reminiscent of a divergence of a relaxation time near a critical point: at $f = 3.43$Hz and $\xi = 0.143$ (blue diamond symbols), the power-law decrease of q_m extends for over 2000 seconds.

Nucleation and phase diagram. To gain further insight into the growth kinetics, we observe the contrast-enhanced grayscale time series micrographs in Figure 7a. The false color images make it clear that the optical density, and hence particle concentration, increases in the vicinity of the voids (indicated by the emergence of red colors). The voids continue to grow, and later, the dense regions form into periodic domains connected by small threads of suspension. Eventually these domains follow the process of forming the zig-zag pattern described above. Comparing Figure 7a and Figure 7b, we see that the nucleation of voids is quicker and growth becomes faster as the duty ratio increases.

The formation of voids is characteristic of nucleation phenomena, and motivates us to compare the perpendicular cluster state points to the phase boundaries estimated by the theoretical thermodynamic equation of state (EoS) and Brownian dynamics simulations for polarizable particles in toggled fields by Sherman et al.[40,44] We interpolate their fluid/fluid (F/F) coexistence binodal and the fluid/solid coexistence boundaries to the value of the magnetic contrast parameter $\beta = (\mu_\mathrm{p}/\mu_\mathrm{f} - 1)/(\mu_\mathrm{p}/\mu_\mathrm{f} + 2) = 0.32$ with μ_p representing the relative magnetic permeability of a particle and μ_f the permeability of the fluid. Further details of the interpolation are provided in the Supporting Information.

The interpolated F/F binodal line for $\beta = 0.32$ is shown in Figure 7c. We estimate that the suspension volume fraction of the suspensions is $\phi \approx 0.45$ based on the bulk volume fraction and the sedimentation height ($\sim 0.1a$) of the colloids.[51] The perpendicular structure state points, then, lie between the F/F (solid line) and F/BCT (dashed line) boundaries. As the duty cycle decreases, the corresponding state points approach the F/BCT line. Conditions where density fluctuation occurs (red closed diamonds) are located below the F/F line, but above F/BCT coexistence line (dashed line). By contrast, conditions for the perpendicular state evolving without the local nucleation (red open diamonds) are located above the F/F

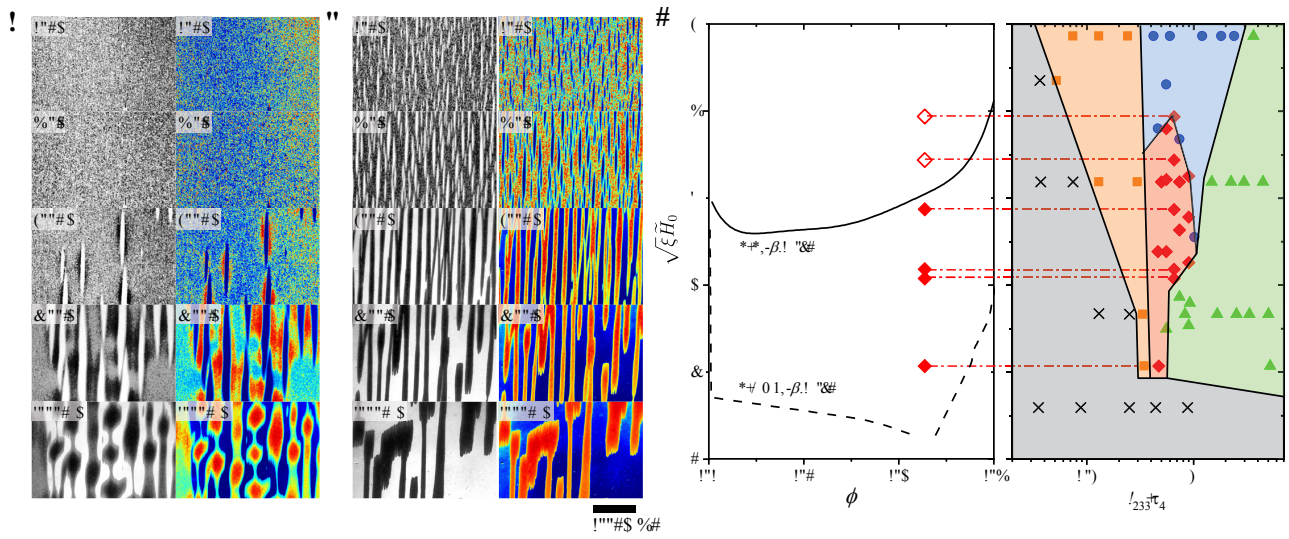

Figure 7: The perpendicular state microstructure (**a**) at $t_{\mathrm{off}}/\tau_{\mathrm{D}} = 0.66$ and $\xi = 0.124$ and (**b**) $t_{\mathrm{off}}/\tau_{\mathrm{D}} = 0.66$ and $\xi = 0.26$ over time are shown with adjusted brightness and enhanced contrast (left panels) and false-color colormap (right panels). (**c**) (Left panel) The F/F and F/BCT coexistence lines are interpolated for $\beta = 0.32$. A black solid line is the interpolated F/F binodal line. The F/BCT coexistence line (dashed line) is also presented. Conditions where the optical fluctuation is observed (i.e. the case shown in **a**) are plotted with closed red diamond symbols and those with no optical fluctuation (i.e. the case shown in **b**) are plotted with open red diamonds. On the right panel, the state diagram shown in Figure 4 is highlighted again with different axis, $\sqrt{\xi}\widetilde{H}_0$ versus $t_{\mathrm{off}}/\tau_{\mathrm{D}}$.

binodal line. This may indicate that magnetic colloidal suspensions exhibit the density fluctuation near the critical point. Additionally, the absence of unique perpendicular pattern formation can be attributed to the limited simulation size scale, which is far smaller than the millimeter-scale perpendicular structure.

Emergent dynamics. After the perpendicular structure reaches a steady state, it exhibits emergent dynamics of a continuous rotating motion, breakup, and coalescence (see the Supporting Movie V1). The rotation is highlighted in Figure 8 by tracking spikes at surface. Here, at $f = 2.2$ Hz and $\xi = 0.22$, the rotational velocity at is 0.71 ± 0.11 μm·s^{-1}. Velocities at different toggling conditions within the perpendicular state boundaries range from 0.71 to 0.87 μm·s^{-1}. Neighboring domains rotate in opposite directions according to their angle with the toggled magnetic field. For instance, in Figure 8, domains oriented from the top-left of the image to the bottom-right rotate clockwise. Neighboring domains oriented from the bottom-left to the top-right rotate counter-clockwise.

The rotational dynamics and the formation of zigzag-patterned structures of colloidal aggregates are similar to instabilities observed for colloidal suspensions in electric fields.[52–57] There are two models that have been proposed to account for the origin of this perpendicular morphology and rotational dynamics: a phase lag between the induced dipole moments and the applied field direction[52,53] and the development of inhomogeneous ion concentrations leading to salt concentration gradients near the aggregates, which in turn induces macroscopic flow.[54–56] The former mechanism is unlikely for paramagnetic colloidal suspension given the rapid Néel relaxation of magnetic moments of magnetic nanoparticles in the order of nanosecond during the field-off stage.[58] But the latter mechanism is also not associated with magnetic colloids.

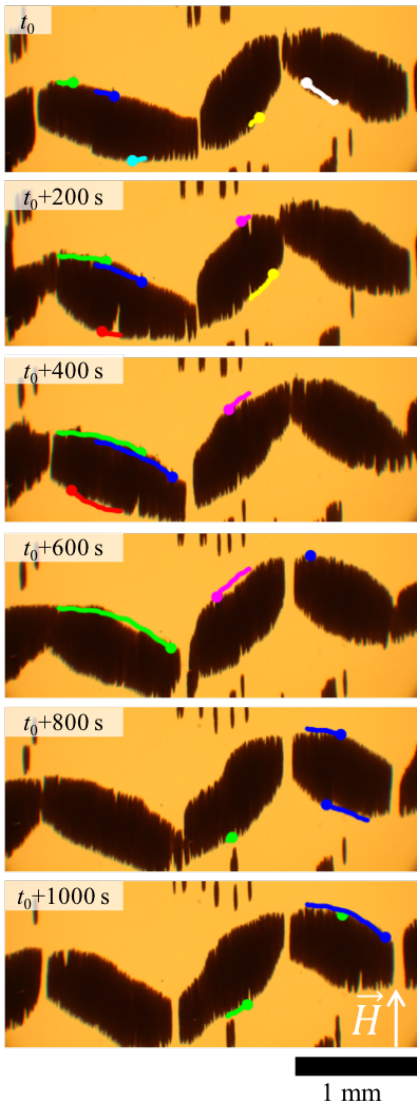

Figure 8: The rotational dynamics of perpendicular microstructures at $f = 2.2$ Hz and $\xi = 0.22$ is highlighted. Spikes on domains are tracked and the traces are presented. The direction of the rotation is towards the colored dot. Scale bar: 1 mm.

Conclusions

We studied the effect of duty ratio on the directed self-assembly of suspension of paramagnetic colloids in toggled magnetic fields. Several structures, including ellipsoid, percolated, and columnar, were observed in earlier studies; the principal effect of the duty ratio is to narrow the ellipsoid phase as the duty ratio decreases. The expanded state diagram is in good agreement with the recent Brownian dynamics simulations and theoretical studies by Sherman and Swan.[40] Computational studies, however, did not identify a new state that we observe over a narrow range of toggling parameters ($1.6 < f < 3.7$ Hz and $0.1 \leq \xi \leq 0.3$): the zigzag-like perpendicular state. The morphological evolution of the perpendicular microstructure is unique and differs from the other states. Particle-empty voids first nucleate and form thick percolated columns. This local nucleation leads to density fluctuations, which then grow orthogonally to the applied field. The structures exhibit emergent dynamics, repeating the continuous breakup into small aggregates and coalescence between the aggregates with rotational dynamics.

While we attempted to understand the perpendicular structure in the context of an interpolated state diagram, clearly the rich kinetics and dynamics of these states deserve further theoretical and computational study. Furthermore, whether the results of this work apply to dispersions of *ferro*magnetic nanoparticles and other dipolar fluids is also of interest, given the large body and long history of work on the subject.[59–61] The ground state structures of magnetic nanoparticles and the structure and topology of particle clusters have been the subject of experimental[62,63] and theoretical studies.[64,65] In such dipolar fluids, the permanent moment of the nanoparticles will likely compete with, and possibly hinder, the field-directing torques and translational forces of a toggled field that ultimately give rise to coarsening and breakup. Such arrest was reported recently in microgravity studies of magnetic ellipsoids in toggled fields.[66] Nonetheless, the response of a wider range of dipolar fluids in toggled fields

deserve further attention, especially given their potential to assemble unique nano- and microstructures.

Supporting Information

State diagrams from the experiments and simulations; interpolation method for the phase diagram (Supporting Information)
Growth of the perpendicular state at frequency $f = 2.47$ Hz and duty ratio $\xi = 0.124$ (Supporting Video V1)

Conflicts of interest

There are no conflicts to declare.

Acknowledgement

The authors thank T. Prileszky and J. Swan for fruitful discussions. Authors acknowledge funding from the NSF (CBET-1637991). M. Sau current address: Department of Chemical Engineering and Materials Science, University of Minnesota, Minneapolis, Minnesota 55455, United States.

References

(1) Grzelczak, M.; Vermant, J.; Furst, E. M.; Liz-Marzán, L. M. Directed self-assembly of nanoparticles. *ACS Nano* **2010**, *4*, 3591–3605.

(2) Prevo, B. G.; Velev, O. D. Controlled, Rapid Deposition of Structured Coatings from Micro- and Nanoparticle Suspensions. *Langmuir* **2004**, *20*, 2099–2107.

(3) Kumnorkaew, P.; Ee, Y.-K.; Tansu, N.; Gilchrist, J. F. Investigation of the Deposition of Microsphere Monolayers for Fabrication of Microlens Arrays. *Langmuir* **2008**, *24*, 12150–12157.

(4) Mittal, M.; Furst, E. M. Electric field-directed convective assembly of ellipsoidal colloidal particles to create optically and mechanically anisotropic thin films. *Advanced Functional Materials* **2009**, *19*, 3271–3278.

(5) Cheng, W.; Wang, J.; Jonas, U.; Fytas, G.; Stefanou, N. Observation and tuning of hypersonic bandgaps in colloidal crystals. *Nature materials* **2006**, *5*, 830–836.

(6) Still, T.; Cheng, W.; Retsch, M.; Sainidou, R.; Wang, J.; Jonas, U.; Stefanou, N.; Fytas, G. Simultaneous Occurrence of Structure-Directed and Particle-Resonance-Induced Phononic Gaps in Colloidal Films. *Phys. Rev. Lett.* **2008**, *100*, 194301.

(7) Beltramo, P. J.; Schneider, D.; Fytas, G.; Furst, E. M. Anisotropic hypersonic phonon propagation in films of aligned ellipsoids. *Physical Review Letters* **2014**, *113*, 1–5.

(8) Park, S. H.; Xia, Y. Macroporous Membranes with Highly Ordered and Three-Dimensionally Interconnected Spherical Pores. *Advanced Materials* **1998**, *10*, 1045–1048.

(9) Jiang, P.; Hwang, K. S.; Mittleman, D. M.; Bertone, J. F.; Colvin, V. L. Template-Directed Preparation of Macroporous Polymers with Oriented and Crystalline Arrays of Voids. *Journal of the American Chemical Society* **1999**, *121*, 11630–11637.

(10) Hatton, B.; Mishchenko, L.; Davis, S.; Sandhage, K. H.; Aizenberg, J. Assembly of large-area, highly ordered, crack-free inverse opal films. *Proceedings of the National Academy of Sciences* **2010**, *107*, 10354–10359.

(11) Velev, O. D.; Kaler, E. W. In Situ Assembly of Colloidal Particles into Miniaturized Biosensors. *Langmuir* **1999**, *15*, 3693–3698.

(12) Xuan, R.; Wu, Q.; Yin, Y.; Ge, J. Magnetically assembled photonic crystal film for

humidity sensing. *J. Mater. Chem.* **2011**, *21*, 3672–3676.

(13) Sanders, J. V. Colour of Precious Opal. *Nature* **1964**, *204*, 1151–1153.

(14) Sanders, J. V. Diffraction of light by opals. *Acta Crystallographica Section A* **1968**, *24*, 427–434.

(15) Pusey, P. N.; van Megen, W. Phase behaviour of concentrated suspensions of nearly hard colloidal spheres. *Nature* **1986**, *320*, 340–342.

(16) Lumsdon, S. O.; Kaler, E. W.; Velev, O. D. Two-Dimensional Crystallization of Microspheres by a Coplanar AC Electric Field. *Langmuir* **2004**, *20*, 2108–2116.

(17) Ding, T.; Song, K.; Clays, K.; Tung, C. H. Fabrication of 3D photonic crystals of ellipsoids: Convective self-assembly in magnetic field. *Advanced Materials* **2009**, *21*, 1936–1940.

(18) Forster, J. D.; Park, J.-G.; Mittal, M.; Noh, H.; Schreck, C. F.; O'Hern, C. S.; Cao, H.; Furst, E. M.; Dufresne, E. R. Assembly of Optical Scale Dumbbells Into Dense Photonic Crystals. *ACS nano* **2011**, 6695–6700.

(19) Mirkin, C. A.; Letsinger, R. L.; Mucic, R. C.; Storhoff, J. J. A DNA-based method for rationally assembling nanoparticles into macroscopic materials. *Nature* **1996**, *382*, 607–609.

(20) Biancaniello, P. L.; Kim, A. J.; Crocker, J. C. Colloidal Interactions and Self-Assembly Using DNA Hybridization. *Phys. Rev. Lett.* **2005**, *94*, 058302.

(21) Kim, A. J.; Biancaniello, P. L.; Crocker, J. C. Engineering DNA-Mediated Colloidal Crystallization. *Langmuir* **2006**, *22*, 1991–2001.

(22) Wang, Y.; Wang, Y.; Zheng, X.; Ducrot, É.; Yodh, J. S.; Weck, M.; Pine, D. J. Crystallization of DNA-coated colloids. *Nature Communications* **2015**, *6*, 7253.

(23) Gast, A. P.; Russel, W. B. Simple Ordering in Complex Fluids. *Physics Today* **1998**, *51*, 24–30.

(24) Zhao, K.; Mason, T. G. Directing Colloidal Self-Assembly through Roughness-Controlled Depletion Attractions. *Phys. Rev. Lett.* **2007**, *99*, 268301.

(25) Promislow, J. H. E.; Gast, A. P.; Fermigier, M. Aggregation kinetics of paramagnetic colloidal particles. *The Journal of Chemical Physics* **1995**, *102*, 5492–5498.

(26) Claesson, E. M.; Philipse, A. P. Monodisperse magnetizable composite silica spheres with tunable dipolar interactions. *Langmuir* **2005**, *21*, 9412–9419.

(27) Fermigier, M.; Gast, A. P. Structure evolution in a paramagnetic latex suspension. *Journal of Colloid and Interface Science* **1992**, *154*, 522 – 539.

(28) Winslow, W. M. Contributed Original Research Induced Fibration of Suspensions. *Journal of Applied Physics* **1949**, *20*, 1137–1140.

(29) Gast, A. P.; Zukoski, C. F. Electrorheological fluids as colloidal suspensions. *Advances in Colloid and Interface Science* **1989**, *30*, 153–202.

(30) Anderson, V. J.; Lekkerkerker, H. N. W. Insights into phase transition kinetics from colloid science. *Nature* **2002**, *416*, 811–815.

(31) Hynninen, A.-P.; Dijkstra, M. Phase Diagram of Dipolar Hard and Soft Spheres: Manipulation of Colloidal Crystal Structures by an External Field. *Phys. Rev. Lett.* **2005**, *94*, 138303.

(32) Furst, E. M. Directed self-assembly. *Soft Matter* **2013**, *9*, 9039–9045.

(33) Promislow, J. H. E.; Gast, A. P. Magnetorheological Fluid Structure in a Pulsed Magnetic Field. *Langmuir* **1996**, *12*, 4095–4102.

(34) Promislow, J. H. E.; Gast, A. P. Low-energy suspension structure of a magnetorheological fluid. *Physical Review E* **1997**, *56*, 642–651.

(35) Swan, J. W.; Vasquez, P. A.; Whitson, P. A.; Fincke, E. M.; Wakata, K.; Magnus, S. H.; Winne, F. D.; Barratt, M. R.; Agui, J. H.; Green, R. D.; Hall, N. R.; Bohman, D. Y.; Bunnell, C. T.; Gast, A. P.; Furst, E. M. Multi-scale kinetics of a field-directed colloidal phase transition. *Proc. Nat. Acad. Sci.* **2012**, *109*, 16023–16028.

(36) Swan, J. W.; Bauer, J. L.; Liu, Y.; Furst, E. M. Directed colloidal self-assembly in toggled magnetic fields. *Soft Matter* **2014**, *10*, 1102.

(37) Sethna, J. P. *Statistical mechanics: entropy, order parameters, and complexity*; Oxford University Press, 2006.

(38) Sherman, Z. M.; Swan, J. W. Dynamic, Directed Self-Assembly of Nanoparticles via Toggled Interactions. *ACS Nano* **2016**, *10*, 5260–5271.

(39) Sherman, Z. M.; Rosenthal, H.; Swan, J. W. Phase Separation Kinetics of Dynamically Self-Assembling Nanoparticles with Toggled Interactions. *Langmuir* **2017**, *34*, 1029–1041.

(40) Sherman, Z. M.; Swan, J. W. Transmutable Colloidal Crystals and Active Phase Separation via Dynamic, Directed Self-Assembly with Toggled External Fields. *ACS Nano* **2019**, *13*, 764–771.

(41) Bauer, J. L.; Liu, Y.; Kurian, M. J.; Swan, J. W.; Furst, E. M. Coarsening mechanics of a colloidal suspension in toggled fields. *J. Chem. Phys.* **2015**, *143*, 074901.

(42) Bauer, J. L.; Kurian, M. J.; Stauffer, J.; Furst, E. M. Suppressing the Rayleigh-Plateau instability in field-directed colloidal assembly. *Langmuir* **2016**, *32*, 6618–6623.

(43) Cutillas, S.; Bossis, G.; Cebers, A. Flow-induced transition from cylindrical to layered patterns in magnetorheological suspensions. *Phys. Rev. E* **1998**, *57*, 804–811.

(44) Sherman, Z. M.; Ghosh, D.; Swan, J. W. Field-Directed Self-Assembly of Mutually Polarizable Nanoparticles. *Langmuir* **2018**, *34*, 7117–7134.

(45) Fiore, A. M.; Swan, J. W. Rapid sampling of stochastic displacements in Brownian dynamics simulations with stresslet constraints. *The Journal of Chemical Physics* **2018**, *148*, 044114.

(46) Promislow, J. H. E.; Gast, A. P. Low-energy suspension structure of a magnetorheological fluid. *Phys. Rev. E* **1997**, *56*, 642–651.

(47) Lele, P. P.; Swan, J. W.; Brady, J. F.; Wagner, N. J.; Furst, E. M. Colloidal diffusion and hydrodynamic screening near boundaries. *Soft Matter* **2011**, *7*, 6844–6852.

(48) Siggia, E. D. Late stages of spinodal decomposition in binary mixtures. *Physical Review A* **1979**, *20*, 595–605.

(49) Furukawa, H. A dynamic scaling assumption for phase separation. *Advances in Physics* **1985**, *34*, 703–750.

(50) Lu, P. J.; Zaccarelli, E.; Ciulla, F.; Schofield, A. B.; Sciortino, F.; Weitz, D. A. Gelation of particles with short-range attraction. *Nature* **2008**, *453*, 499–503.

(51) Chen, S.-H.; Huang, J. S.; Tartaglia, P. *Structure and dynamics of strongly interacting colloids and supramolecular aggregates in solution*; Springer Netherlands, 1992; Vol. 369.

(52) Hu, Y.; Glass, J. L.; Griffith, A. E.; Fraden, S. Observation and simulation of electrohydrodynamic instabilities in aqueous colloidal suspensions. *The Journal of Chemical Physics* **1994**, *100*, 4674–4682.

(53) Kiriyama, T.; Ozawa, T.; Akimoto, T.; Yoshimura, H.; Mitsui, T. Conditions for Self-Organization of 45° Vortex and Phase Lag in Electric Polarization. *Japanese Journal of Applied Physics* **1997**, *36*, 7282–7288.

(54) Isambert, H.; Ajdari, A.; Viovy, J.-L.; Prost, J. Electrohydrodynamic Patterns in Charged Colloidal Solutions. *Phys. Rev. Lett.* **1997**, *78*, 971–974.

(55) Isambert, H.; Ajdari, A.; Viovy, J.-L.; Prost, J. Electrohydrodynamic patterns in macroion dispersions under a strong electric field. *Phys. Rev. E* **1997**, *56*, 5688–5704.

(56) Ladoux, B.; Isambert, H.; Léger, J.-F.; Viovy, J.-L. New Rectifying Electrohydrodynamic Instability at the Boundary of Charged Gels in Alternating Electric Fields. *Phys. Rev. Lett.* **1998**, *81*, 3793–3796.

(57) Lele, P. P.; Mittal, M.; Furst, E. M. Anomalous Particle Rotation and Resulting Microstructure of Colloids in AC Electric Fields. *Langmuir* **2008**, *24*, 12842–12848.

(58) Néel, L. Theory of ferromagnetic magnetic drag grained application with terrocotta. *Ann. Geophys* **1949**, *5*, 99–136.

(59) Sear, R. P.; Jackson, G. Thermodynamic perturbation theory for association into chains and rings. *Phys. Rev. E* **1994**, *50*, 386–394.

(60) Teixeira, P. I. C.; Tavares, J. M.; da Gama, M. M. T. The effect of dipolar forces on the structure and thermodynamics of classical fluids. *Journal of Physics: Condensed Matter* **2000**, *12*, R411–R434.

(61) Wang, Z.; Holm, C.; Müller, H. W. Molecular dynamics study on the equilibrium magnetization properties and structure of ferrofluids. *Phys. Rev. E* **2002**, *66*, 021405.

(62) Butter, K.; Bomans, P. H. H.; Frederik, P. M.; Vroege, G. J.; Philipse, A. P. Direct observation of dipolar chains in iron ferrofluids by cryogenic electron microscopy. *Nature Materials* **2003**, *2*, 88–91.

(63) Klokkenburg, M.; Erné, B. H.; Mendelev, V.; Ivanov, A. O. Magnetization behavior of ferrofluids with cryogenically imaged dipolar chains. *Journal of Physics: Condensed Matter* **2008**, *20*, 204113.

(64) Kantorovich, S. S.; Ivanov, A. O.; Rovigatti, L.; Tavares, J. M.; Sciortino, F. Temperature-induced structural transitions in self-assembling magnetic nanocolloids. *Phys. Chem. Chem. Phys.* **2015**, *17*, 16601–16608.

(65) Rovigatti, L.; Kantorovich, S.; Ivanov, A. O.; Tavares, J. M.; Sciortino, F. Branching points in the low-temperature dipolar hard sphere fluid. *The Journal of Chemical Physics* **2013**, *139*, 134901.

(66) Kim, H.; Bauer, J. L.; Vasquez, P. A.; Furst, E. M. Structural coarsening of magnetic ellipsoid particle suspensions driven in toggled fields. *Journal of Physics D: Applied Physics* **2019**, *52*, 184002.

Graphical TOC Entry